# Analysis of Shock Motion in STBLI Using DNS Data

M. Wu*and M.P. Martin†

*Mechanical and Aerospace Engineering Department*

*Princeton University, Princeton, NJ 08540*

**Direct numerical simulation data of a 24° compression ramp configuration are used to analyze the shock motion. The motion can be observed from the animated DNS data and from wall-pressure and mass-flux signals measured in the free stream. The characteristic low frequency is in the range of 0.007-0.013 $U_\infty/\delta$, as found in Wu & Martin.[1] The shock motion also exhibits high-frequency of $O(U_\infty/\delta)$, small-amplitude spanwise wrinkling , which is mainly caused by the spanwise nonuniformity of turbulent structures in the incoming boundary layer. In studying the low frequency streamwise oscillation, conditional statistics show that there is no significant difference in the properties of the incoming boundary layer when the shock location is upstream or downstream. The spanwise-mean separation point also undergoes a low frequency motion and is found to highly correlate with the shock motion. A small correlation is found between the low-momentum structures in the incoming boundary layer and the separation point. Correlations among the spanwise-mean separation point, reattachment point and the shock location indicate that the low-frequency shock unsteadiness is influenced by the downstream flow. Preliminary analyses of an 12° reflected shock configuration DNS are also presented.**

## I. Introduction

The boundary layer flow over a compression ramp is one of the canonical shock wave and turbulent boundary layer interaction (STBLI) configurations that have been studied extensively in experiments since the 1970's. From this body of work, we have learned that the shock motion has a frequency much lower than the characteristic frequency of the incoming boundary layer. The time scale of the low frequency motion is $O(10\delta/U_\infty - 100\delta/U_\infty)$ as reported in various experiments such as Dolling & Or,[2] Selig,[3] Dussauge et al.,[4] and Dupont et al.[5] In contrast, the characteristic time scale of the incoming boundary layer is $O(\delta/U_\infty)$. The scale to normalize the frequency of the shock is still under debate. However, Dussauge et al.[4] found that using $St_L = fL/U_\infty$, where $L$ is the streamwise length of the separation bubble, experimental data (covering a wide range of Mach numbers and Reynolds numbers and various configurations) can be grouped between $St_L = 0.02$ and 0.05. Also, the cause of the low frequency motion is still a research question. Plotkin[6] proposed a damped spring model for the shock motion. Andreopoulos & Muck[7] concluded that the shock motion is driven by the bursting events in the incoming boundary layer. However, Thomas et al.[8] found no connection between the shock motion and bursting events in the incoming boundary layer. Erengil et al.[9] found that there was a correlation between certain shock motions with pressure fluctuations in the incoming boundary layer. Beresh et al.[10] found that positive velocity fluctuations near the wall correlate with downstream shock motion. Pirozzoli et al.[11] analyzed DNS data of a reflected shock interaction and proposed that a resonance mechanism might be responsible for the shock unsteadiness. Dussauge et al.[4] suggested that the three-dimensional nature of the interaction in the reflected shock configuration is a key to understanding the shock unsteadiness. Ganapathisubramani et al.[12] proposed that very long alternating structures of uniform low- and high-speed fluid in the logarithmic region of the incoming boundary layer are responsible for the low frequency motion of the shock. These so called 'superstructures' have been

*Graduate Student, AIAA Student Member.

†Assistant Professor, AIAA Senior Member.

observed in supersonic boundary layers by Sammimy et al.[13] and are also evident in the elongated wall-pressure correlation measurements of Owen & Horstmann.[14] Superstructures have also been observed in the atmospheric boundary layer experiments of Hutchins & Marusic[15] and confirmed in DNS of supersonic boundary layers by Ringuette et al.[16]

Wu & Martin[1] presented a direct numerical simulation of STBLI for a 24° compression ramp configuration at Mach 2.9 and Reynolds number based on momentum thickness of 2300. They validated the DNS data against the experiments of Bookey et al.[17] at matching flow conditions, and they illustrated the existence of the superstructures. In this paper, we use the Wu & Martin[1] data to analyze the shock unsteadiness. While in previous experiments the shock motion is usually inferred by measuring the wall pressure, our analyses of the shock motion are carried mainly in the outer part of the boundary layer and in the free stream. This is because the Reynolds number that we consider is much lower than those in typical experiments. In turn, viscous effects are more prominent, the shock does not penetrate as deeply as in higher Reynolds number flows, and the shock location is not well-defined in the lower half of the boundary layer. In addition, the motion of the separation bubble is studied. Table I lists the inflow boundary layer conditions, and Figure 1 shows the computational domain and the coordinate system. Notice that we use $z_{\rm n}$ to denote the wall-normal coordinate and prime symbols to denote fluctuating quantities. Statistics are gathered over $300\delta/U_\infty$. The characterization of the shock motion and the unsteadiness of the separation bubble are given in Sections II and III. Preliminary DNS data of the 12° reflected shock interaction are presented in Section IV. A discussion of the shock motion is presented in Section V. Finally, conclusions are drawn in Section VI.

| $M$ | $Re_\theta$ | $\theta$ (mm) | $\delta^*$ (mm) | $\delta$ (mm) | $\delta^+$ | $C_f$ |
|---|---|---|---|---|---|---|
| 2.9 | 2300 | 0.38 | 1.80 | 6.4 | 320 | 0.0021 |

**Table 1. Inflow conditions for the DNS. The Mach number, Reynolds number based on the momentum thickness, displacement thickness, boundary layer thickness, boundary layer thickness in wall variables, and skin friction are given in order of appearance.**

## II. Shock motion

Figure 2(a) plots three wall-pressure signals measured at three streamwise locations upstream of the ramp corner (the corner is located at $x = 0$) along the spanwise center line. In the incoming boundary layer at $x = -6.9\delta$, the normalized magnitude is around one with small fluctuations. At $x = -2.98\delta$, which is the mean separation point (defined as the point where the mean skin friction coefficient changes sign from positive to negative), the magnitude fluctuates between 1 to 1.2. At $x = -2.18\delta$, the magnitude oscillates between 1.5 and 2. The corresponding premultiplied energy spectra are plotted in Figure 2(b). At the mean separation point, the peak frequency is $0.007U_\infty/\delta$. At $x = -2.18$, the peak is in 0.01 $U_\infty/\delta$. Let us define the Strouhal number $St = fL/U_\infty$, where $L$ is the separation length ($L = 4.2\delta$ in the DNS). The range of $St_L$ is 0.03-0.042, which is consistent with the range given by.[4]

Contours of the magnitude of the gradient of pressure on streamwise-spanwise planes are plotted in Figure 3. Two instantaneous flow fields are plotted at $z_{\rm n} = 0.9\delta$ and $2\delta$ away from the wall. At $z_{\rm n} = 0.9$, Figures 3(a) and (b), the shock is nearly uniform in the spanwise direction. The streamwise movement of the shock is roughly $1\delta$. Figures 3(c) and (d) plot the same times at a plane closer to the wall. We observe a wrinkling of the shock in the spanwise direction, with an amplitude of about $0.5\delta$. At $z_n = 0.9\delta$, the shock also moves in the streamwise direction in the same manner as shown in Figures 3(a) and (b). The amplitude of the motion in the streamwise direction is twice that of the spanwise wrinkling.

We analyze the shock motion within the context of these two aspects. One is that the shock wrinkles along the spanwise direction. The other corresponds to the larger amplitude motion upstream and downstream. The motion that is inferred from the wall-pressure signal in Figure 2 results from the combination of these two aspects. However, the low frequency motion is related to the large-amplitude, streamwise motion rather than to the spanwise wrinkling. This can be seen from the mass-flux signals measured in the free stream as shown in Figure 4. The signals are measured at different streamwise locations (upstream, inside, and

downstream of the shock motion region) with a distance of $2\delta$ away from the wall along the centerline of the computational domain. In Figure 4(a), the mass-flux signal measured inside the region of shock motion oscillates between those measured upstream and downstream, indicating that the shock is moving upstream and downstream of that point. The premultiplied energy spectra plotted in Figure 4(b) show that the characteristic low frequency range is between $0.007 - 0.013 U_\infty/\delta$, which is roughly the same as that given by the wall-pressure signals in Figure 2(b).

Figure 5 plots normalized iso-surfaces of $|\nabla\rho|$ for four consecutive instantaneous flow fields. The structures in the incoming boundary layer and the shock are seen. Two structures are highlighted in Figures 5(a) and 5(c). For an adiabatic wall, as in the DNS, these structures contain low-density, low-speed fluid. As these structures pass through the shock, the shock curves upstream, resulting in spanwise wrinkling of the shock as shown in Figures 5(b) and (d). From the data animation, the characteristic frequency of spanwise wrinkling is $O(U_\infty/\delta)$.

To analyze the unsteadiness, we introduce two definitions for the averaged shock location. First, the spanwise-mean location, $SK_{\rm sm}$, in which the instantaneous location is defined as the point where the pressure rises to $1.3p_\infty$ in the streamwise direction. Thus, $SK_{\rm sm}$ is a function of time and $z_{\rm n}$. Second, the absolute mean shock location, $SK_{\rm m}$, which is computed by spanwise and temporal averaging the instantaneous shock location. In turn, $SK_{\rm m}$ is only a function of $z_{\rm n}$. Figure 3 (b) and (d) show $SK_{\rm sm}$ and $SK_m$ locations.

The correlation with time lag between the pressure at $SK_{\rm sm}$ and the mass flux in the undisturbed incoming boundary layer ($5\delta$ upstream of the ramp corner) is plotted in Figure 6(a). Using $SK_{\rm sm}$ in the correlation removes the effect of the streamwise motion. The local correlation is computed first using data on spanwise planes and then the local correlations are spanwise averaged. The signals are sampled at $z_{\rm n} = 0.7\delta$ since the shock is well defined there. A peak of the correlation is observed at $\tau = -3.3\delta/U_\infty$ (i.e. events are separated about $3\delta$) with a magnitude of about 0.35. The "enhanced" correlation is also plotted in the same figure, where the contribution to the correlation is only computed whenever the difference between the instantaneous shock location and $SK_{\rm sm}$ is greater than $0.15\delta$ (or 1.5 standard deviations). In other words, only strong events are accounted for. The enhanced correlation has a similar shape to the regular correlation. It peaks at the same location with a greater magnitude, indicating that the correlation is mainly influenced by strong events. Thus, the spanwise wrinkling is related to low momentum fluid.

Figure 6(b) plots the correlation between pressure at the absolute mean shock location, $SK_{\rm m}$, and the mass flux in the undisturbed incoming boundary layer. For the regular correlation, a peak is observed at the same location as in Figure 6(a), but with a much smaller magnitude. The enhanced correlation is also computed, using data only when the instantaneous shock location deviates from $SK_{\rm m}$ more than $0.3\delta$ (or 1.5 standard deviations). Again, the enhanced correlation peaks at the same location, however, the magnitude observed is still much smaller than those in Figure 6(a). Measuring the mass flux of the incoming boundary layer in the logarithmic region, where the superstructures are best identified, gives equally low correlation values. Thus, the streamwise shock motion is not significantly affected by low momentum structures in the incoming boundary layer. Computing the correlations in Figure 6 without spanwise averaging gives the same result except that the correlation curve is not as smooth due to the lesser number of samples.

Conditional statistics on the incoming boundary layer have been calculated, conditionally based on the shock being upstream or downstream of the absolute mean location. No significant difference is found in these properties. The conditionally averaged mean profiles and boundary layer parameters (Table I) are nearly identical with very small difference (consistently less than 3%). This is in agreement with the experiments of Beresh et al.[10] for a 28° compression ramp with $M = 5$, where the difference in the conditionally averaged mean velocity was roughly 2%.

## III. Unsteadiness of the separation bubble

The separation and reattachment points (denoted by $S$ and $R$, respectively) are defined using a $C_f = 0$ criteria. Figure 7 (a) plots the time evolution of the spanwise-mean separation point $S_{\rm sm}$ and the reattachment point $R_{\rm sm}$. The spectra for these signals also exhibit a low frequency component of about $0.01\ U_\infty/\delta$. The shock foot is related to the separation point because the flow turns first near the separation bubble. Thus, we expect a strong correlation between $S_{\rm sm}$ and $SK_{\rm sm}$. Figure 7 (b) plots the correlation for the spanwise-mean separation point $S_{\rm sm}$ and $SK_{\rm sm}$ at $z_{\rm n} = 2\delta$. The correlation peak is about 0.85 with a time lag of about $7\delta/U_\infty$. Notice the time interval between each data point in Figure 7 (b) is about $3\delta/U_\infty$, therefore the peak location has $\pm 3\delta/U_\infty$ uncertainty. This uncertainty also applies for all of the follow-

ing correlations with time lag.[18] correlated the instantaneous separation point $S$ (defined using a velocity threshold criteria) and streamwise-averaged values of streamwise velocity in the incoming boundary layer at $z_n = 0.2\delta$. The same analysis performed here yields a correlation of about 0.5, which is similar to the value 0.4 found by Ganapathisubramani et al.[18] Figure 8a plots the profile for the correlation between the instantaneous separation point using the $C_f = 0$ definition and streamwise-averaged values of $\rho u$, where the streamwise averaging is performed from the separation point to the inlet. Using the $C_f = 0$ criteria, the correlation factor at $z_n = 0.2$ is 0.23. Thus, the use of the actual definition of the separation point decreases the correlation between the separation point and the streamwise-averaged $u$ significantly.

Figure 8b plots two correlations, the correlation between $S_{sm}$ and $R_{sm}$ and the correlation between the shock location $SK_{sm}$ and $R_{sm}$ For the correlation between $S_{sm}$ and $R_{sm}$, a negative correlation is observed, indicating that the separation bubble undergoes a contraction/expansion motion. Moreover, the peaks for both correlations are located at negative time lags, indicating that the motion of the separation point (and the shock) lags that of the reattachment point. This implies that the shock unsteadiness may be caused by the flow inside the separation region, downstream of the shock.

## IV. Preliminary Data of the Reflected Shock Interaction

Using the same numerical method and boundary conditions as Wu & Martin,[1] an 12° reflected shock interaction DNS is also being preformed. The computation domain is shown in Figure 9. At the inlet, jump conditions are imposed to generate the impinging shock. The domain size in the spanwise direction is $2.2\delta$. The recycling station for the rescaling method is located at $4.5\delta$ downstream of the inlet.

Figure 10 plots the instantaneous density gradient contours for the reflected shock interaction. The triple point is located at a wall-normal location of about $2\delta$ at this instant. Similar to the compression ramp interaction, density gradient is seen amplified downstream of the interaction. Figure 11 plots the mean wall-pressure distribution compared with the reference experiments of Bookey et al.[17] under the same flow conditions. The DNS result is computed using current available data. Large differences are observed between the DNS result and the experimental data points. Three-dimensional effects in the experiments are believed to be responsible for the differences. More specifically, the reflected shock interaction is observed to be highly three-dimensional in experiments due to side-wall effects, as shown in Figure 12. The mean wall-pressure distribution is measured along the center line of Figure 12, where the size of the separation bubble is the largest ($10.5\delta$ in length). In the DNS, the mean separation and reattachment points are located at $x = 6.9\delta$ and $x = 14.4\delta$, respectively, so that the separation length is $7.5\delta$ in the DNS.

Three wall-pressure signals of the reflected shock interaction are plotted in Figure 13. The signal measured at $x = 2\delta$ shows very small variation around 1. The signal measured at $x = 5.9\delta$ rises around $t = 250\delta/U_\infty$ and drops around $t = 320\delta/U_\infty$ and remains around 1 thereafter. The last signal, which is measured at $x = 7.1\delta$, also drops around $t = 320\delta/U_\infty$ and then remains at a low value thereafter, with small amplitude oscillations visible. From the wall-pressure signals measured in this $200\delta/U_\infty$ period, then the low frequency shock motion is not well resolved using the current available data. If we believe that the low frequency shock motion scales with the length of the separation bubble $L$ and $U_\infty$, it can be inferred using the compression ramp DNS data that the frequency of the slow shock motion should be about 0.004-0.007 $U_\infty/\delta$ in the reflected shock interaction, which means that the time scale of the low frequency motion can be as large as 250 $\delta/U_\infty$.

## V. Discussion

The DNS data show that the low-frequency shock motion is a streamwise displacement of the shock that is nearly uniform in the spanwise direction. To investigate the effect of domain size, a DNS with a $4\delta$ spanwise domain has been performed. Figure 14a shows that the instantaneous shock structure is similar to that of the case with a $2\delta$ spanwise domain. This result does not exclude the possibility of large-wavelength, low-frequency spanwise shock wrinkles, as it is sketched in Figure 14. If that were the case, from the DNS results one can infer that these events must have a large spanwise extent (larger than $4\delta$).

Figure 15 shows sequential planform images from filtered Rayleigh scattering of Mach 2.5 flow over a 24° wedge at $Re_\theta$=14,000 from the experiments of Wu[19] and Wu & Miles.[20] The images are taken at $z_n = 0.9\delta$. The frame size corresponds to $4\delta \times 4\delta$, and the frame rate is 500 kHz, corresponding to about $5U_\infty/\delta$. In this time scale a structure upstream (enclosed by the circle in the first frame) flows through

the shock wave. The resulting, low-amplitude spanwise wrinkling of the shock by the passing of the eddy is apparent. In addition, a large-amplitude, large-wavelength spanwise wrinkle can be observed in all frames, with characteristic wavelength greater than $4\delta$. These experimental visualizations are in agreement with the DNS data analyses.

Regarding the causes of the shock unsteadiness, the local spanwise wrinkling shock motion is shown to correlate with low momentum fluid in the incoming boundary layer, which is consistent with what Wu & Miles[20] found in a compression ramp interaction using high speed visualization techniques. However, the spanwise wrinkling is a smaller scale, local unsteadiness compared with the streamwise shock motion. The small correlation between the low momentum fluid in the incoming boundary layer and the separation point found in the DNS implies that these low momentum structures might have a relatively minor contribution to the shock unsteadiness. The negative time lag in the correlation between the shock location and reattachment point suggests that the separation region may play an important role in driving the low frequency shock unsteadiness, as seen experimentally by Thomas et al.[8] The fact that the Strouhal number of the low frequency shock motion defined using the separation length lies in the experimental range (Dussauge et al.[4]) is also supportive for this argument. Pirozzoli et al.[11] performed a DNS of a reflected shock interaction and proposed that the shock unsteadiness was sustained by an acoustic resonance mechanism that is responsible for generating tones in cavity flows. However, the low-frequency shock motion may not be captured in their DNS due to the fact that the lowest Strouhal number reported is between 0.09 and 0.24, which is above the range 0.02-0.05 found in experiments. According to Dussauge et al.,[4] the Strouhal number of the low frequency motion does not seem to have a significant dependence on Mach number, suggesting that acoustic resonance may not cause the low-frequency shock motion. It is interesting to point out that in cavity flows, there are two modes observed (Gharib & Roshko;[21] Rowley et al.[22]): the shear-layer mode and the wake mode. In this case, acoustic resonance is responsible for the generation of the shear-layer mode, while the wake mode is purely hydrodynamic. Moreover, the wake mode corresponds to larger scale and lower frequency motions compared to the shear-layer mode. Providing that there are some similarities in compression ramp interactions and cavity flows in that they all have a shear layer formed above a separated region, we suggest that the mechanism of the low-frequency shock unsteadiness may resemble that of the generation of the wake mode in cavity flows. In other separated flows, for example, flow passing a backward-facing step, low frequency fluctuations have also been indicated (e.g. Simpson[23]), while the driving mechanisms are still not fully understood.

DNS data animations show that the size (including the length and height) of the separation bubble changes significant with a low frequency that is comparable to that of the low frequency shock motion. Figure 16 plots six consecutive times in the DNS with time intervals of about $\delta/U_\infty$, showing the break down of the separation bubble indicated by streamlines. Flow quantities are averaged in the spanwise direction to get a clear picture. Contours of pressure gradient are also plotted to show the shock location. From frame (c) to (f), fluid bursts outside the separation bubble, causing the bubble to shrink.

The shock then moves downstream at a later time (not seen in the figure). To show how the separation bubble changes with time, the mass and the area of reverse flow region inside the separation bubble are plotted in Figure 17(a). The reverse flow region is defined as regions in which $u$ is negative, where $u$ is spanwise averaged. It is observed that the mass inside the reverse flow region has an intermittent character, just like the momentum signal inside the shock motion region show in Figure 4. Figure 17(b) plots the correlation of the mass signal with the spanwise averaged shock location at $z = 2\delta$. A high peak of 0.7 is observed at about $\tau = -13\delta/U_\infty$, showing the shock motion is closely related to that of the separation bubble. In addition, the shock motion lags that of the separation bubble, indicating that the separation bubble drives the shock motion. Also, Figure 17(b) plots the correlation of the mass signal with the pressure difference between $x = 1\delta$ and $x = -2\delta$, which are close to the reattachment and separation points, respectively. The pressure gradient decreases with increasing mass of reverse flow, which is due to the enlargement of the separation bubble in the streamwise direction and decreasing of streamline curvature.

Based on the above observations, it is hypothesized that one of the mechanisms driving the low-frequency shock motion can be described as a feedback loop between the separation bubble, the separated shear layer and the shock system, which has some similarities with the cause of the low-frequency "flapping motion" in backward-facing step flows described by Eaton & Johnston.[24] That is, the balance between shear layer entrainment from the separation bubble and injection near the reattachment point is perturbed. If the injection is greater, the separation bubble grows in size and causes the reattachment point to move downstream and the separation point to move upstream. The motion of the separation point causes the shock

to move with it. As the shock moves upstream, the pressure gradient in the separation region decreases due to the enlargement of the separation region and decreasing of streamline curvature. The decreasing pressure gradient reduces the entrainment of fluid into the separation bubble. In turn, the separation bubble becomes unstable and breaks down. When this happens, fluid bursts outside the bubble and the separation region shrinks fairly rapidly, causing the shock to move downstream at a later time. Similarly, when the shock moves to a downstream location, the overall pressure gradient in the separation region increases, which enhances entrainment of fluid into the separation bubble, causing the bubble to grow. Thus, the low frequency shock motion is closely related to the time scale associated with the growth and burst of the separation bubble. Assuming that this time scale is determined by the length of the separation bubble $L$ and the characteristic speed of the reverse flow $U_R$, the dimensionless shock frequency $St_R = fL/U_R$ can be computed. Using the maximum of the time-averaged reverse flow speed in the separation bubble, $0.055U_\infty$, to represent $U_R$, the dimensionless frequency $St_R$ in the DNS is around unity (about 0.8).

## VI. Conclusion

Wall-pressure and separation point signals indicate low-frequency motions in DNS data of a 24° compression ramp. Analyses show that the shock motion is characterized by a low-frequency, large-amplitude streamwise motion with characteristic frequency of about $0.013U_\infty/\delta$, and a relative smaller-amplitude, high-frequency $O(U_\infty/\delta)$ spanwise wrinkling. The mass flux in the incoming boundary layer is correlated with the high-frequency spanwise wrinkling motion. Conditional statistics indicate no significant difference in the mean properties of the incoming boundary layer when the shock is upstream/downstream.

The location of the separation point is highly correlated with shock location with a time lag of about $7\delta/U_\infty$. A small correlation is found between the low momentum structures in the incoming boundary layer and the separation point, indicating the influence of the superstructures on the shock motion may be minor. However, it is found that both the shock motion and the separation point motion are correlated with and lag the motion of the reattachment point, suggesting that the downstream flow plays an important role in driving the low frequency shock motion. A model that is described as a feedback loop between the separation bubble, the separated shear layer, and the shock system is proposed to explain the low frequency shock motion. Using the length of the separation bubble and the characteristic reverse flow speed (e.g. the maximum of the mean reverse flow speed), the Strouhal number of the low frequency shock motion is around unity.

## acknowledgments

We would like to acknowledge insightful discussions with Prof. A.J. Smits and the support from the Air Force Office of Scientific Research under grant no. AF/9550-06-1-0323.

## References

[1]Wu, M. and Martin, M. P., "Direct Numerical Simulation of Shockwave and Turbulent Boundary Layer Interaction induced by a Compression Ramp," *AIAA Journal*, Vol. 45, No. 4, 2007, pp. 879–889.

[2]Dolling, D. S. and Or, C. T., "Unsteadiness of the Shock Wave Structure in Attached and Separated Compression Ramp Flows," *Experiments in Fluids*, Vol. 3, No. 1, 1985, pp. 24–32.

[3]Selig, M. S., *Unsteadiness of Shock Wave/Turbulent Boundary Layer Interactions with Dynamic Control*, Ph.D. thesis, Princeton University, 1988.

[4]Dussauge, J. P., Dupont, P., and Devieve, J. F., "Unsteadiness in Shock Wave Boundary Layer Interactions with Separation," *Aerospace Science and Technology*, Vol. 10, No. 2, 2006.

[5]Dupont, P., Haddad, C., and Debieve, J., "Space and time organization in a shock-induced separated boundary layer," *Journal of Fluid Mechanics*, Vol. 559, 2006, pp. 255–277.

[6]Plotkin, K., "Shock wave oscillation driven by turbulent boundary-layer fluctuations," *AIAA Journal*, Vol. 13, No. 8, 1975, pp. 1036–1040.

[7]Andreopoulos, J. and Muck, K. C., "Some New Aspects of The Shock-wave/Boundary-layer Interaction in Compression-ramp Flows," *Journal of Fluid Mechanics*, Vol. 180, July 1987, pp. 405–428.

[8]Thomas, F. O., Putnam, C. M., and Chu, H. C., "One the Mechanism of Unsteady Shock Oscillation in Shock Wave/Turbulent Boundary Layer Interactions," *Experiments in Fluids*, Vol. 18, 1994, pp. 69–81.

[9]Erengil, M. E. and Dolling, D. S., "Correlation of Separation Shock Motion with Pressure Fluctuations in the Incoming Boundary Layer," *AIAA Journal*, Vol. 29, No. 11, 1991, pp. 1868–1877.

[10]Beresh, S. J., Clemens, N. T., and Dolling, D. S., "Relationship Between Upstream Turbulent Boundary-Layer Velocity Fluctuations and Separation Shock Unsteadiness," *AIAA Journal*, Vol. 40, No. 12, 2002, pp. 2412–2423.

[11]Pirozzoli, S. and Grasso, F., "Direct Numerical Simulation of Impinging Shock Wave/Turbulent Boundary Layer Interaction at $M = 2.25$," *Physics of Fluids*, Vol. 18, No. 6, 2006.

[12]Ganapathisubramani, B., Clemens, N. T., and Dolling, D. S., "Planar Imaging Measurements to Study The Effect of Spanwise Structure of Upstream Turbulent Boundary Layer on Shock Induced Separation," *AIAA Paper No. 2006-324*, Jan. 2006.

[13]Samimy, M., Arnette, S. A., and Elliott, G. S., "Streamwise Structures in a Turbulent Supersonic Boundary Layer," *Physics of Fluids*, Vol. 6, No. 3, 1994, pp. 1081–1083.

[14]Owen, F. and Horstmann, C., "On the structure of hypersonic turbulent boundary layers," *Journal of Fluid Mechanics*, Vol. 53, 1972, pp. 611–636.

[15]Hutchins, N. and Marusic, I., "Evidence of very long meandering features in the logarithmic region of turbulent boundary layers," *Journal of Fluid Mechanics. In Press*, 2007.

[16]Ringuette, M. J., Wu, M., and Martin, M. P., "Coherent Structures in DNS of Supersonic Turbulent Boundary Layers at Mach 3," *Under consideration in Journal of Fluid Mechanics. Also AIAA Paper No. 2007-1138*, 2007.

[17]Bookey, P. B., Wyckham, C., Smits, A. J., and Martin, M. P., "New Experimental Data of STBLI at DNS/LES Accessible Reynolds Numbers," *AIAA Paper No. 2005-309*, Jan. 2005.

[18]Ganapathisubramani, B., Clemens, N. T., and Dolling, D. S., "Effects of Upstream Coherent Structures on Low-Frequency Motion of Shock-Induced Turbulent Separation," *AIAA Paper No. 2007-1141*, Jan. 2007.

[19]Wu, P., *MHz-Rate Pulse-Burst Laser Imaging System: Development and Application in the High-Speed Flow Diagnostics*, Ph.D. thesis, Princeton University, 2000.

[20]Wu, P. and Miles, R., "Megahertz Visualization of Compression-Corner Shock Structures," *AIAA Journal*, Vol. 39, No. 8, August 2001, pp. 1542–1546.

[21]Gharib, M. and Roshko, A., "The Effect of Flow Oscillations on Cavity Drag," *Journal of Fluid Mechanics*, Vol. 177, Apr. 1987, pp. 501–530.

[22]Rowley, C. W., Colonius, T., and Basu, A. J., "On Self-Sustained Oscillation in Two-Dimensional Compressible FLow over Rectangular cavities," *Journal of Fluid Mechanics*, Vol. 455, Mar. 2002, pp. 315–346.

[23]Simpson, R. L., "Turbulent Boundary-Layer Separation," *Annual Review of Fluid Mechanics*, Vol. 21, 1989, pp. 205–234.

[24]Eaton, J. K. and Johnston, J. P., "Low-Frequency Unsteadiness of a Reattaching Turbulent Shear Layer." *Proceedings of the 3rd International symposium on Turbulent Shear Flow*, Springer, Berlin Heidelberg New York, 1981.

[25]Wu, M. and Martin, M. P., "Analysis of shock motion in shockwave/turbulent boundary layer interaction using DNS data," *submitted to Journal of Fluid Mechanics*, 2007.

[26]Bookey, P., *An Experimental Study of Shock/Turbulent Boundary Layer Interactions at DNS Accessible Reynolds Numbers*, Master's thesis, Princeton University, 2005.

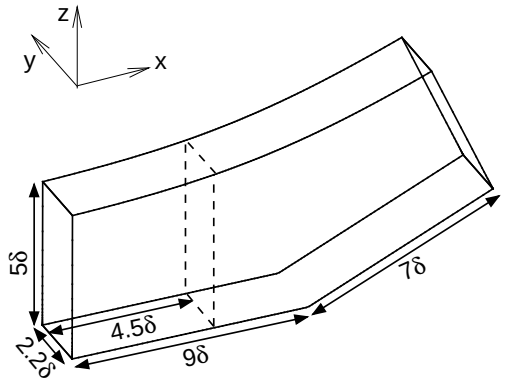


**Figure 1. Computational domain of the DNS and coordinate system.**

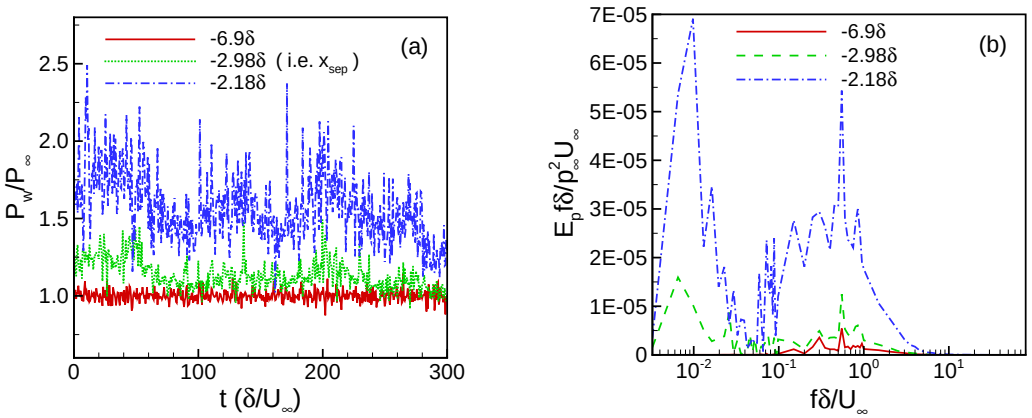


**Figure 2. (a) Wall-pressure signals and (b) wall-pressure energy spectra at different streamwise locations relative to the ramp corner with $y = 1.1\delta$. From Wu & Martin.[1]**

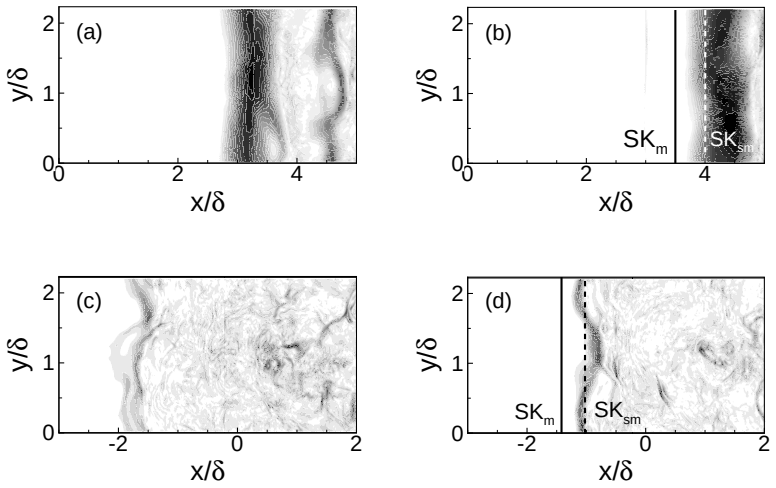


**Figure 3. Contours of $|\nabla p|$ showing the shock location for two flow realizations separated by $50\delta/U_\infty$ at $z_\mathrm{n} = 2\delta$ ((a) & (b)) and $z_\mathrm{n} = 0.9\delta$ ((c) & (d)). Dark indicates large gradient. From Wu & Martin.[25]**

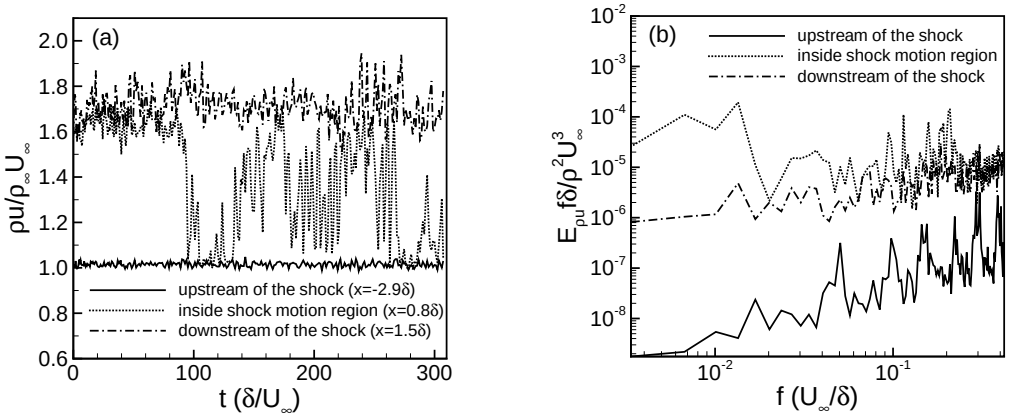


**Figure 4. (a) Mass-flux signals and (b) corresponding premultiplied energy spectra measured for different streamwise locations at $z_\mathrm{n} = 2\delta$. From Wu & Martin[1]**

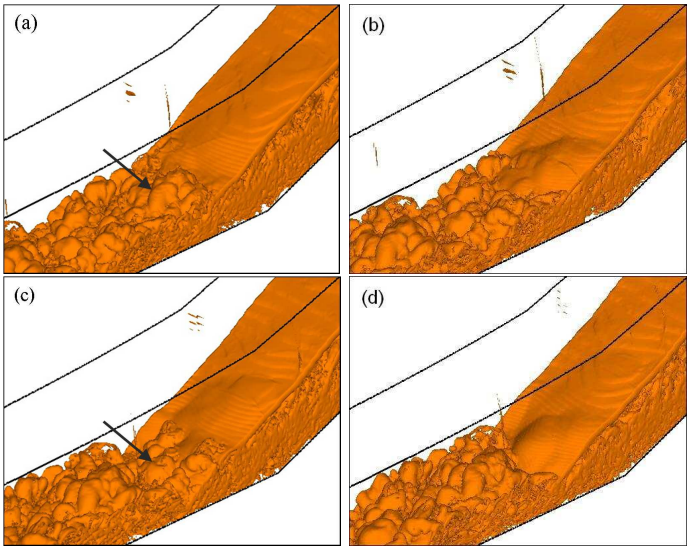


**Figure 5. Iso-surface of $|\nabla\rho| = 2\rho_\infty/\delta$ showing structures in the incoming boundary layer passing through the shock. Temporal spacing between each frame is $\delta/U_\infty$. From Wu & Martin.[25]**

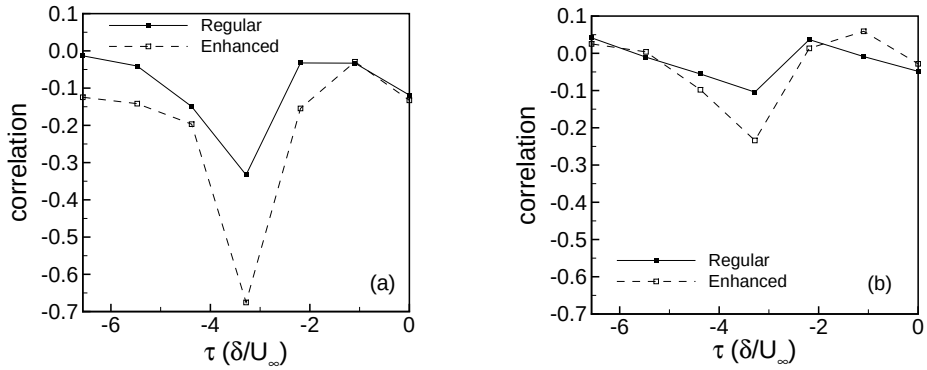


**Figure 6. Spanwise-averaged correlation with time lag between (a) mass flux at ($x = -5\delta$, $y$, $z_\mathrm{n} = 0.7\delta$) and pressure at ($SK_\mathrm{sm}$, $y$, $z_\mathrm{n} = 0.7\delta$), and (b) mass flux at ($x = -5\delta$, $y$, $z_\mathrm{n} = 0.7\delta$) and pressure at ($SK_\mathrm{m}$, $y$, $z_\mathrm{n} = 0.7\delta$). From Wu & Martin.[25]**

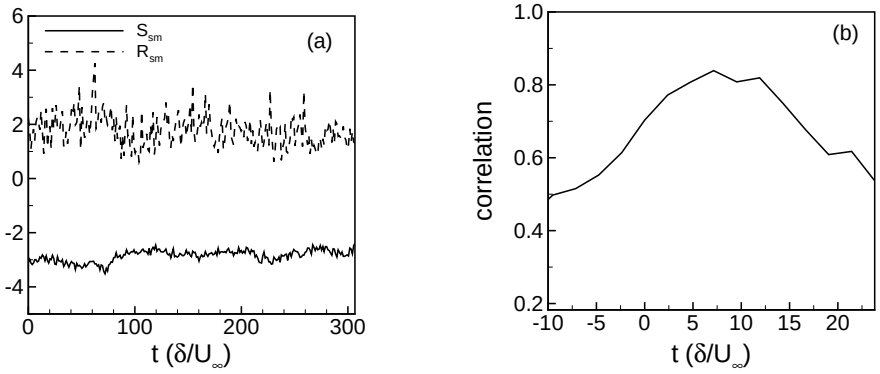


**Figure 7. (a) Time evolution of the spanwise-mean separation and reattachment points and (b) correlation between the spanwise-mean separation point $S_\mathrm{sm}$ and shock location $SK_\mathrm{sm}$ at $z_\mathrm{n} = 2\delta$. From Wu & Martin.[25]**

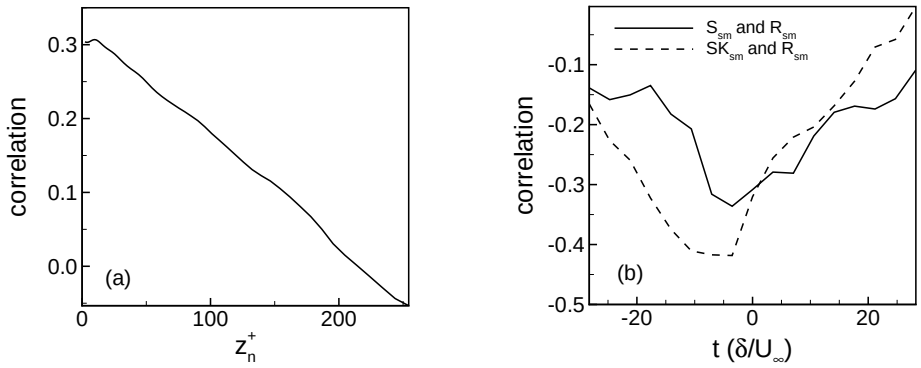


**Figure 8. (a) Correlation profile between the instantaneous separation point and streamwise averaged values of $\rho u$ and (b) correlation between the separation and reattachment point and the shock location at $z_n = 2$ and the reattachment point. From Wu & Martin.[25]**

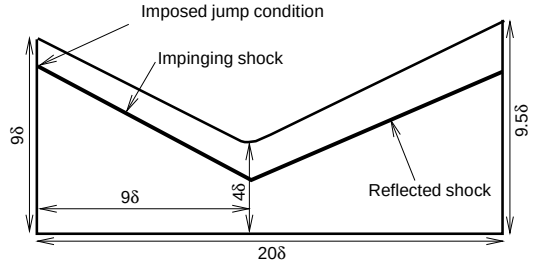


**Figure 9. Computational domain of the 8° reflected shock interaction.**

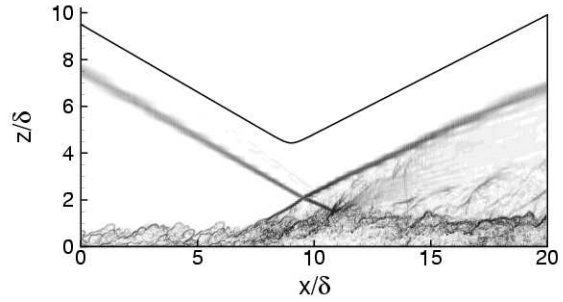


**Figure 10. Instantaneous density gradient contours for the 8° reflected shock interaction.**

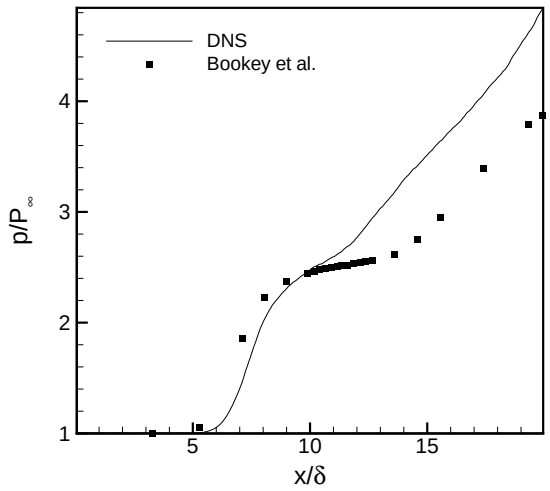


**Figure 11. Comparison of the mean wall-pressure distribution between DNS and the reference experiments for the reflected shock configuration.**

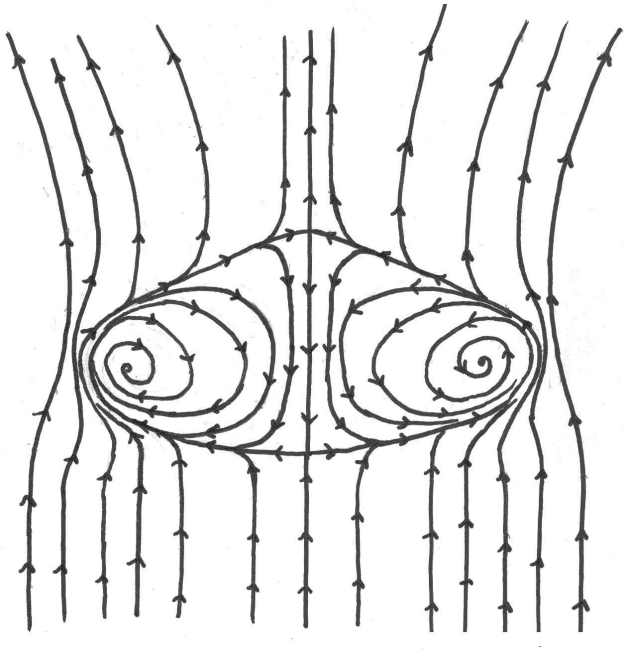

**Figure 12. Schematic of the surface flow pattern for the reflected shock configuration at Mach 2.9. From Bookey.[26]**

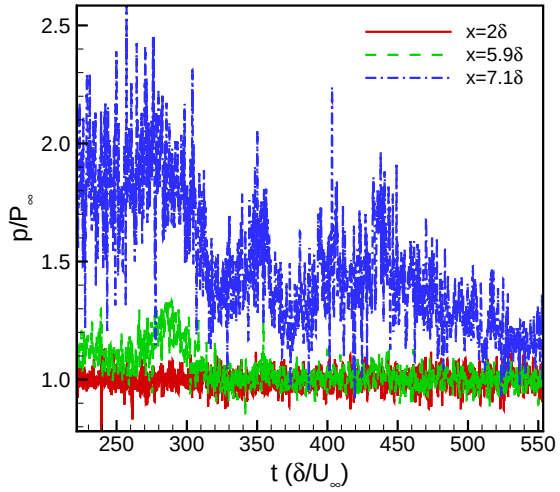


**Figure 13. Wall-pressure signals for the reflected shock interaction.**

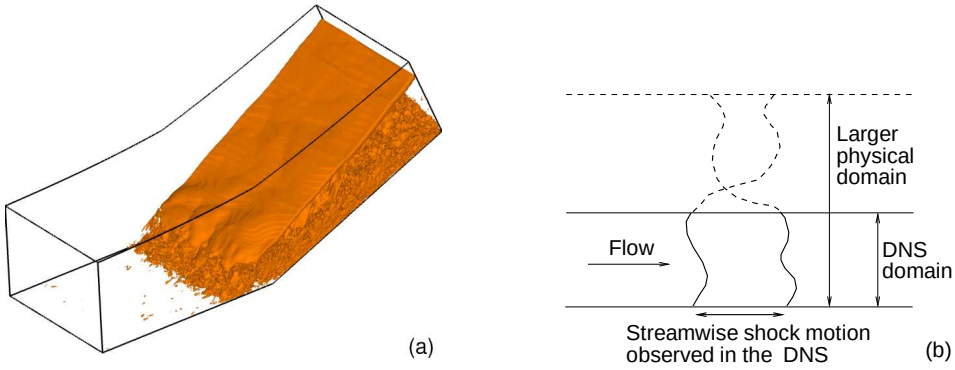


**Figure 14. (a) $|\nabla p| = 0.5 p_\infty/\delta$ showing the structure of the shock in the $4\delta$ spanwise domain DNS case and (b) sketch of possible shock motion pattern in a domain with a larger spanwise extent. From Wu & Martin.[25]**

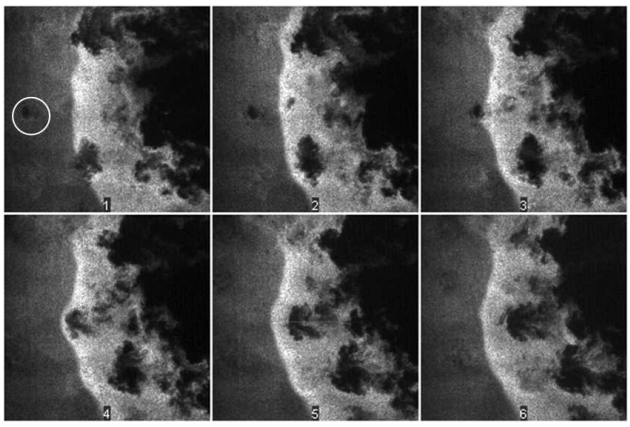

**Figure 15. Sequential planform images at $z_n = 0.9\delta$ from filtered Rayleigh scattering of Mach 2.5 flow over 24° wedge at $Re_\theta = 14,000$ from the experiments of Wu[19] and Wu & Miles.[20] Printed with permission.**

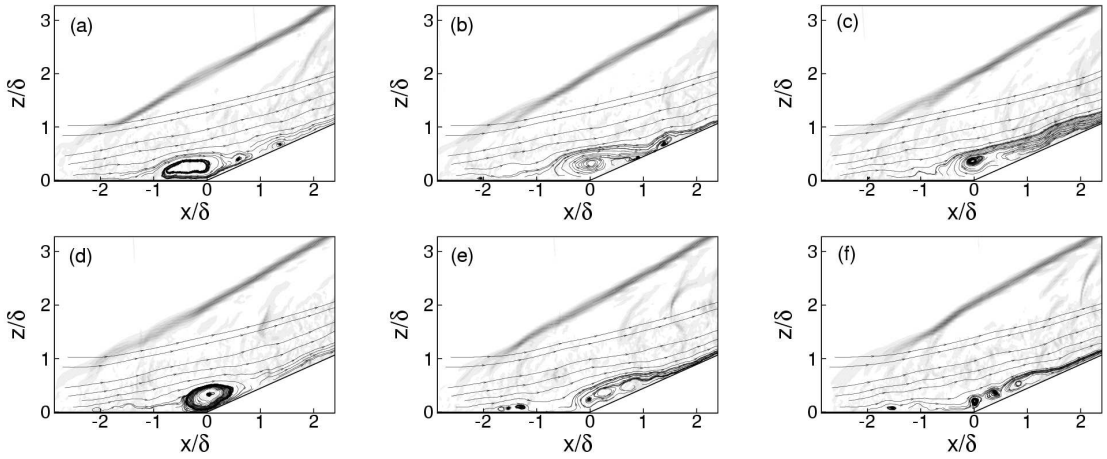


**Figure 16. Streamlines in $x-z$ planes showing break down of the separation bubble. Time intervals are about $1\delta/U_\infty$. From Wu & Martin.[25]**

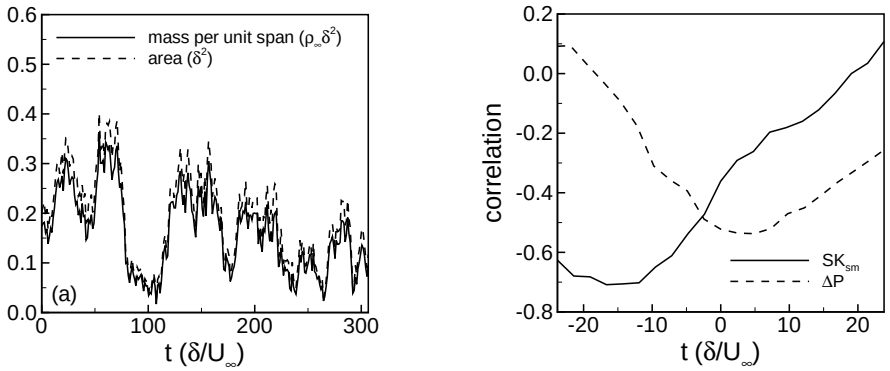


**Figure 17. (a) Mass and volume of the reverse flow region versus time and (b) Correlation between the mass inside the reverse flow region with the spanwise mean shock location $SK_{\rm sm}$ at $z = 2\delta$ and with the wall pressure difference $\Delta P = P_w(x = 1\delta) - P_w(x = -2\delta)$. From Wu & Martin.[25]**